

# Luttinger compensated magnetic material $\text{LaMn}_2\text{SbO}_6$

Xiao-Yao Hou<sup>1,2</sup>, Ze-Feng Gao<sup>1,2</sup>, Huan-Cheng Yang<sup>1,2,\*</sup>, Peng-Jie Guo<sup>1,2,†</sup> and Zhong-Yi Lu<sup>1,2,3‡</sup>

1. School of Physics and Beijing Key Laboratory of Opto-electronic Functional

Materials & Micro-nano Devices. Renmin University of China, Beijing 100872, China

2. Key Laboratory of Quantum State Construction and Manipulation (Ministry of Education),

Renmin University of China, Beijing 100872, China and

3. Hefei National Laboratory, Hefei 230088, China

(Dated: April 15, 2025)

Unconventional magnetism including altermagnetism and Luttinger compensated magnetism, characterized by its duality of real-space antiferromagnetic alignment and momentum-space spin splitting, has garnered widespread attention. While altermagnetism has been extensively studied, research on Luttinger compensated magnetism remains very rare. In particular, Luttinger compensated magnetic materials are only theoretically predicted and have not yet been synthesized experimentally. In this study, based on symmetry analysis and the first-principles electronic structure calculations, we predict that  $\text{LaMn}_2\text{SbO}_6$  is a Luttinger compensated magnetic semiconductor. Given that the Mn ions at opposite spin lattice cannot be connected by any symmetry, the spin splitting in  $\text{LaMn}_2\text{SbO}_6$  is isotropic. More importantly,  $\text{LaMn}_2\text{SbO}_6$  has already been synthesized experimentally, and its magnetic structure has been confirmed by neutron scattering experiments. Therefore,  $\text{LaMn}_2\text{SbO}_6$  serves as an excellent material platform for investigating the novel physical properties of Luttinger compensated magnetic materials.

*Introduction.* Conventionally, magnetism is usually divided into two major categories: ferromagnetism and antiferromagnetism. Ferromagnetic materials have non-relativistic spin-polarized splitting electronic band structures due to breaking time-reversal symmetry ( $T$ ) and have been used widely in spintronic devices. However, the devices based on ferromagnetic materials experience several shortcomings: (i) they are easily affected by the external magnetic field and temperature, (ii) the information storage density is low, and (iii) the device speed is relatively slow (GHz magnitude). In contrast, the information storage density of antiferromagnetic materials can reach the atomic level, and the device speed based on antiferromagnetic materials can be up to THz range. However, the spin polarization of antiferromagnetism is negligible because of its zero net magnetic moment, which means that antiferromagnetism is inefficient in generating and transmitting spin polarized currents, which is not conducive to the performance improvement of spintronic devices. The desirable materials for next generation spintronic devices should take the advantages of both ferromagnetic and antiferromagnetic materials.

Recently, altermagnetism, as a newly discovered third type of magnetism, has attracted a great deal of attention in the field of magnetism[1–4]. In altermagnetic materials, the opposite spin sublattices cannot be connected by space-inversion symmetry and fractional translation symmetry, but by rotation or mirror symmetry. Altermagnet has time-reversal symmetry-breaking responses and spin polarization phenomena, such as the giant magnetoresistance (GMR) effect[5, 6], the anomalous Hall effect

(AHE)[7], the quantum anomalous Hall effect (QHE)[8], and so on. Moreover, several altermagnetic materials have been confirmed experimentally[9, 10].

Although altermagnetism has the advantages of both ferromagnetism and antiferromagnetism, it has to be admitted that because the crystal field anisotropy of magnetic atoms with opposite spins is usually weak in altermagnetic materials, the spin splitting is correspondingly small[11], which brings difficulties to practical applications. This motivates the search for Luttinger compensated magnetic materials. In Luttinger compensated magnetism, two opposite spin sublattices cannot be connected by any symmetry operation, resulting in isotropic spin splitting just like ferromagnetism, but the net magnetic moment is still zero just like antiferromagnetism according to Luttinger's theorem[12–14]. Although several Luttinger compensated magnetic materials have been theoretically predicted, none of these materials have been synthesized experimentally[15, 16].

In this study, based on symmetry analysis and the first-principles electronic band structure calculations, we predicted  $\text{LaMn}_2\text{SbO}_6$  is a Luttinger compensated magnetic semiconductor. Due to the absence of any symmetry connecting the Mn atoms with opposite magnetic moments,  $\text{LaMn}_2\text{SbO}_6$  exhibits isotropic  $s$ -wave spin splitting. Moreover, under spin-orbit coupling (SOC), the top of valence bands of  $\text{LaMn}_2\text{SbO}_6$  still largely maintain complete spin polarization. The Néel temperature of  $\text{LaMn}_2\text{SbO}_6$  is estimated to be around 50K by Monte Carlo simulation.

*Computational method.* The structural optimization and electronic structure calculation of  $\text{LaMn}_2\text{SbO}_6$  were studied in the framework of density functional theory (DFT) [17–19] by using the Vienna Ab initio Simulation Package (VASP) [20–22]. The core electrons as well as the interaction between the core and valence electrons

\* hcyang@ruc.edu.cn

† guopengjie@ruc.edu.cn

‡ zlu@ruc.edu.cn

were described by using the projector augmented-wave method [23]. The generalized gradient approximation (GGA) of Perdew-Burke-Ernzerhof (PBE) [24] type was adopted as the exchange-correlation functional, using an energy cut-off of 600 eV for the plane waves. A  $6 \times 6 \times 6$  Monkhorst-Pack  $k$  mesh was used for the Brillouin zone (BZ) sampling of the unit cell. The internal atomic positions were fully relaxed until the forces on all atoms were smaller than 0.01 eV/Å. In order to take into account the correlation effects of Mn 3d orbitals, we carried out GGA+U [25] calculations employing the simplified rotationally invariant version proposed by Dudarev et al. [26]. The onsite effective  $U_{eff}$  value of Mn 3d electrons in  $\text{LaMn}_2\text{SbO}_6$  was choose as 3.8 eV. The Monte Carlo simulations based on the classical Heisenberg model were conducted by making use of the open source project MCSOLVER [27].

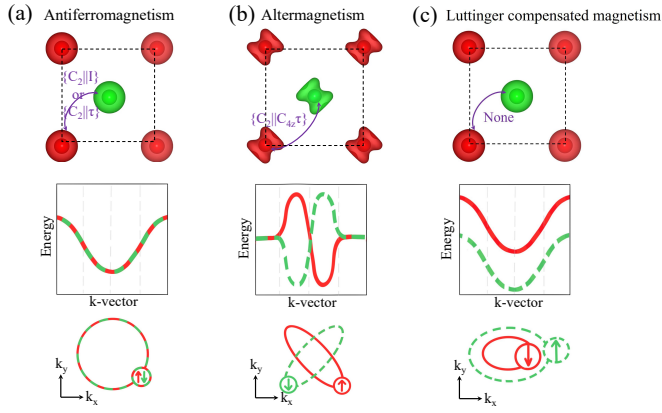


FIG. 1. Schematic diagrams of the three types of compensated magnetism. (a) antiferromagnetism, (b) altermagnetism, (c) Luttinger compensated magnetism. The upper, middle, and lower panels in (a), (b), and (c) represent the polarized charge density, band structure, and Fermi surface, respectively. The red and green represent spin-up and spin-down channels, respectively.

**Results.** Based on spin group symmetry, collinear compensated magnetism can be classified into three categories as shown in Fig. 1. The first category is conventional collinear antiferromagnetism, whose sublattices with opposite spin moments are connected by  $\{C_2||I\}$  or  $\{C_2||\tau\}$  spin symmetry (Fig. 1(a)), where  $I$  and  $\tau$  represent space-inversion and fractional translation operations, respectively. These symmetries enforce Kramers degeneracy throughout the entire BZ, thus conventional collinear antiferromagnetic materials have spin-degenerate electronic bands without spin-orbit coupling (SOC) as shown in Fig. 1(a). The second category is altermagnetism. In altermagnetism, the sublattices with opposite spin moments cannot be connected by  $\{C_2||I\}$  and  $\{C_2||\tau\}$  spin symmetry but by  $\{C_2||R\}$  or mirror  $\{C_2||M\}$  spin symmetries (Fig. 1(b)), which guarantees zero total magnetic moment. The breaking of  $\{C_2||I\}$  and  $\{C_2||\tau\}$  lifts Kramers degeneracy, leading to band

structure with anisotropic spin splitting without SOC (Fig. 1(b)). The third category is the Luttinger compensated magnetism, where the opposite spin sublattices are not connected by any symmetry (Fig. 1(c)). Therefore, the electronic band structure is isotropic  $s$ -wave spin splitting without SOC (Fig. 1(c)). Compared to altermagnetism, Luttinger compensated magnetism has not yet been experimentally confirmed. Here, we aim to predict Luttinger compensated magnetic materials among the materials that have already been synthesized.

$\text{LaMn}_2\text{SbO}_6$  has been reported as a doubly ordered perovskite structure (also reported as double-double perovskite, DDPv) with space group  $P4_2/n$  (No. 86). The elementary symmetry operations of the  $P4_2/n$  space group are  $C_{4z}(\frac{1}{2}, \frac{1}{2}, \frac{1}{2})$  and  $I(\frac{1}{2}, \frac{1}{2}, \frac{1}{2})$ , resulting in the point group  $C_{4h}$ . A schematic diagram of the unit cell is shown in Fig. 2(a), which combines the columnar (Mn and La atoms) and rock-salt (Mn and Sb atoms) orders of 1:1 cations, respectively. The corresponding BZ together with the high-symmetry points and high-symmetry lines are shown in Fig. 2(b).

In  $\text{LaMn}_2\text{SbO}_6$ , the Mn atoms are respectively located in octahedral, tetrahedral, and square planar crystal fields, which are correspondingly labeled as A, B, and C as shown in Fig. 2(c). Due to the complexity of the atomic structure of  $\text{LaMn}_2\text{SbO}_6$ , we considered ten magnetic configurations to check the magnetic ground state of  $\text{LaMn}_2\text{SbO}_6$  as shown in Fig. 2(c) - 2(l). Our calculations show that the total energy of the AFM1 magnetic state is always the lowest among the ten magnetic configurations with the variation of correlation interaction (Fig. 3(a)). Therefore, the AFM1 state is the magnetic ground state of  $\text{LaMn}_2\text{SbO}_6$ , which is consistent with the results of neutron scattering experiment [28, 29]. The AFM1 state is intra-layer ferromagnetic and inter-layer antiferromagnetic (Fig. 2(c)) and the magnetic primitive cell for AFM1 state is the same as the crystal primitive cell. So  $\text{LaMn}_2\text{SbO}_6$  has no  $\{C_2||\tau\}$  symmetry. Furthermore, our symmetry analysis reveals that all symmetry operations in the nonsymmorphic  $C_{4h}$  point group can only connect the Mn ions with the same spin moments for  $\text{LaMn}_2\text{SbO}_6$ . Thus, the Mn ions with opposite spin moments can not be connected by any symmetry. Therefore,  $\text{LaMn}_2\text{SbO}_6$  may be a Luttinger-compensated magnetic material.

On the other hand, the magnetic transition temperature is a very important feature for magnetic materials. To estimate the Néel temperature of  $\text{LaMn}_2\text{SbO}_6$ , we begin by considering a classical Heisenberg model that includes the first- and second-nearest-neighbor exchange interactions as a try. The exchange interaction parameters  $J_1$  and  $J_2$  can be obtained by mapping the energies of three distinct magnetic structures onto the tentative Heisenberg model. Specifically, we select the ground-state AFM1 configuration along with any two of AFM2, AFM3, AFM5, and AFM6. These four magnetic configurations closely resemble the ground state magnetic configuration AFM1. Our calculations reveal that the

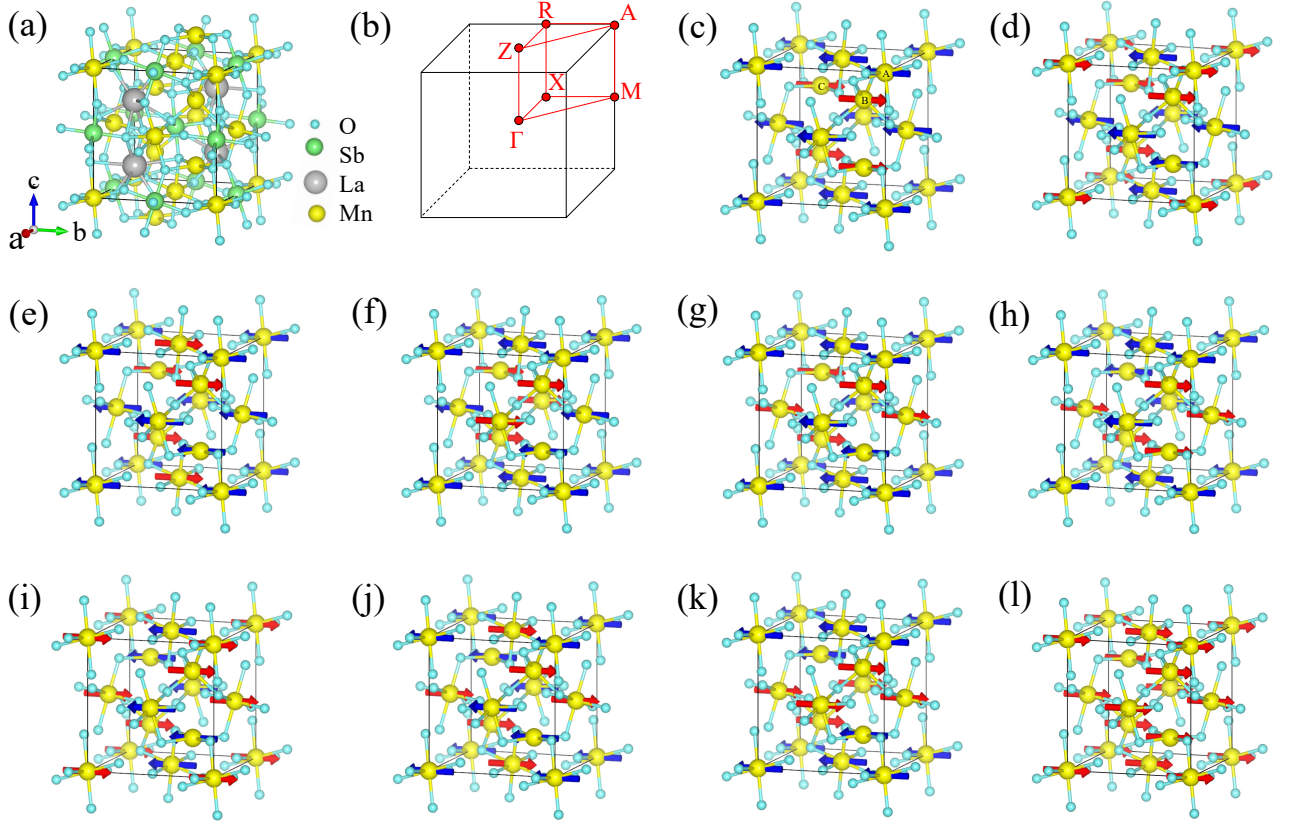


FIG. 2. (a) Nonmagnetic crystal structure of  $\text{LaMn}_2\text{SbO}_6$ . (b) The corresponding bulk Brillouin zone, the high-symmetry points and paths are marked by red dots and lines. (c-k) nine trial AFM configurations. (l) FM configuration.

magnitude of  $J_1$  is approximately two orders larger than that of  $J_2$ . Thus,  $J_2$  is negligible, we adopt a first-nearest-neighbour 3D cubic lattice classical Heisenberg model :

$$H = -J_1 \sum_{\langle i,j \rangle} S_i S_j \quad (1)$$

where  $S_{i(j)}$  represents the spin of  $\text{Mn}^{2+}$  ion on site  $i(j)$ .  $J_1$  denote the first-nearest exchange interaction parameter between  $\text{Mn}(a)$  and  $\text{Mn}(b)$ . Mapping the energies of the ground state magnetic configuration AFM1 and AFM6 onto the above Heisenberg model yields  $J_1 S^2$ . The values of  $J_1 S^2$  for different  $U$  values are presented in Table 1. As illustrated in Figure 3(c), the Néel temperature of  $\text{LaMn}_2\text{SbO}_6$  can be extracted from the peak of the specific-heat capacity based on the Monte Carlo simulations. When  $U=3.8$  eV, the simulated Néel temperature is 48.99 K, which closely aligns with the experimental value ( $\sim 48$  K)[28].

Next, we study the electronic properties of  $\text{LaMn}_2\text{SbO}_6$  with the correlation interaction  $U$  set at 3.8 eV. Without SOC,  $\text{LaMn}_2\text{SbO}_6$  is a direct bandgap semiconductor with bandgap being 1.57 eV, and its spin-up and spin-down bands are completely split. This is due to the absence of any symmetry connecting Mn ions with opposite magnetic moments.

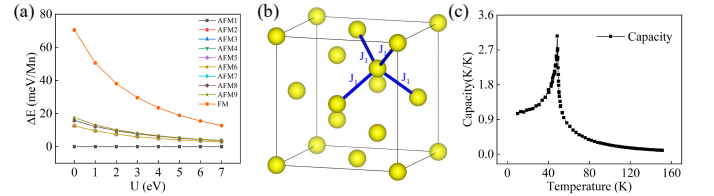


FIG. 3. (a) Relative energies of eight trial AFM and the FM states with respect to the AFM1 state at different  $U$  values. (b) The blue lines represent the first-nearest neighbors. (c) The evolution of specific heat capacity with temperature of  $\text{LaMn}_2\text{SbO}_6$ .

From Fig. 4(a), the valence bands of  $\text{LaMn}_2\text{SbO}_6$  exhibit significant spin splitting, while the conduction bands show relatively smaller spin splitting. We speculate that the valence bands of  $\text{LaMn}_2\text{SbO}_6$  are primarily contributed by the 3d orbitals of Mn atoms, while the conduction bands are mainly contributed by non-magnetic atoms. To confirm this, we plotted the band structure of  $\text{LaMn}_2\text{SbO}_6$  with orbital weights as shown in Fig. 4(b). From Fig. 4(b) the valence bands of  $\text{LaMn}_2\text{SbO}_6$  are indeed mainly contributed by the 3d orbitals of Mn, while the conduction bands are primarily

TABLE I. The values of  $J_1S^2$  at different  $U$  values.

$U$ (eV)	0	1	2	3	4	5	6	7
$J_1S^2$ (K)	-145.71	-110.91	-87.00	-69.99	57.46	-47.43	-39.89	-33.63

contributed by Sb atoms. On the other hand, we also calculated the polarized charge density distribution of  $\text{LaMn}_2\text{SbO}_6$ . Although the Mn atoms are respectively in octahedral, tetrahedral, and square planar crystal fields of O atoms, the polarized charge densities of all Mn ions are approximately spherical, which reflects that all Mn are half filled and in high-spin state. The calculated magnetic moment on every Mn is about  $4.6 \mu_B$ , indicating strong Hund's interactions among Mn 3d electrons. Therefore, the orbital magnetic moments are quenched well in  $\text{LaMn}_2\text{SbO}_6$ . Additionally, since  $\text{LaMn}_2\text{SbO}_6$  is a semiconductor with identical electrons for spin-up and spin-down, its total spin magnetic moment should be zero according to the Luttinger theorem[12–14]. Thus,  $\text{LaMn}_2\text{SbO}_6$  is a Luttinger compensated magnetic material with robust zero net magnetic moment.

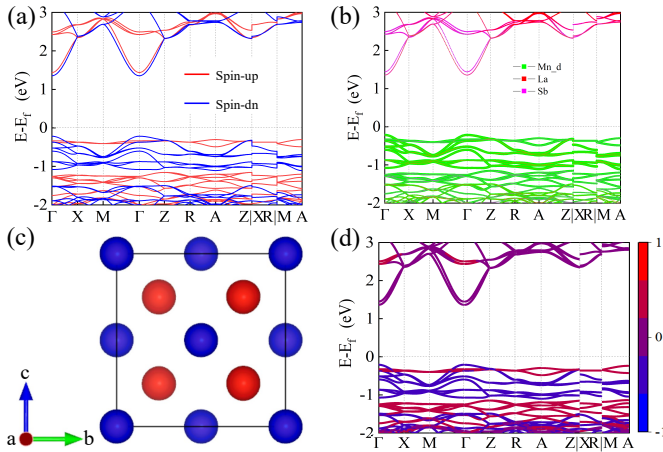


FIG. 4. (a) The electronic band structure without SOC at  $U_{eff} = 3.8$  eV. (b) The corresponding fat band without SOC. (c) The spin-polarized density for spin-up (red) and spin-down (blue). (d) The electronic band structure with SOC at  $U_{eff} = 3.8$  eV.

When SOC is taken into account, the calculations of magnetic anisotropy indicate that the easy magnetization axis of  $\text{LaMn}_2\text{SbO}_6$  is in the  $xy$  plane. Therefore, we have plotted the band structure with  $S_y$  projections as shown in Fig. 4(d). Although SOC does not lead to significant changes for the bands, it does cause noticeable

alterations for polarization of bands. From Fig. 4(d), the spin polarization of the bottom of conduction bands has changed significantly, which is attributed to the fact that these conduction bands are primarily contributed by the Sb atomic orbitals with strong SOC. In contrast, the valence bands, which are mainly contributed by the 3d orbitals of Mn atoms with weak SOC, still largely maintain complete spin polarization. If hole doping is performed,  $\text{LaMn}_2\text{SbO}_6$  will not only generate a net spin current but also retain its semiconducting properties. Moreover,  $\text{LaMn}_2\text{SbO}_6$  can avoid the disadvantage of stray fields caused by non-zero magnetic moments in ferromagnetic semiconductors. Therefore,  $\text{LaMn}_2\text{SbO}_6$  may be very advantageous for the research of new electronic devices.

**Summary.** Based on symmetry analysis and the first-principles electronic structure calculations, we have systematically investigated the magnetic and electronic properties of  $\text{LaMn}_2\text{SbO}_6$ . The calculated ground state magnetic structure is consistent with the results of neutron scattering experiments, and the electronic structure calculations show that  $\text{LaMn}_2\text{SbO}_6$  is a Luttinger compensated magnetic semiconductor with a 1.57 eV band gap. Due to the absence of any symmetry connecting Mn atoms with opposite magnetic moments,  $\text{LaMn}_2\text{SbO}_6$  exhibits isotropic  $s$ -wave spin splitting. Moreover, under SOC, the valence bands of  $\text{LaMn}_2\text{SbO}_6$  still largely maintain complete spin polarization.  $\text{LaMn}_2\text{SbO}_6$  is an excellent material platform for studying the novel physical properties of Luttinger compensated magnetism.

## ACKNOWLEDGMENTS

This work was financially supported by the National Natural Science Foundation of China (Grant No.12204533, No.12434009 and No.62476278), the National Key R&D Program of China (Grant No. 2024YFA1408601), the Fundamental Research Funds for the Central Universities, and the Research Funds of Renmin University of China (Grant No. 24XNKJ15). Computational resources have been provided by the Physical Laboratory of High Performance Computing at Renmin University of China.

[1] S. Hayami, Y. Yanagi, and H. Kusunose, Momentum-Dependent Spin Splitting by Collinear Antiferromagnetic Ordering, *J. Phys. Soc. Jpn.* **88**, 123702 (2019).

[2] L. Šmejkal, R. González-Hernández, T. Jungwirth, and J. Sinova, Crystal time-reversal symmetry breaking and spontaneous Hall effect in collinear antiferromagnets, *Sci.*



- Adv.* **6**, eaaz8809 (2020).
- [3] L.-D. Yuan, Z. Wang, J.-W. Luo, E. I. Rashba, and A. Zunger, Giant momentum-dependent spin splitting in centrosymmetric low- $Z$  antiferromagnets, *Phys. Rev. B* **102**, 014422 (2020).
  - [4] I. I. Mazin, K. Koepernik, M. D. Johannes, R. González-Hernández, and L. Šmejkal, Prediction of unconventional magnetism in doped FeSb<sub>2</sub>, *Proc. Natl. Acad. Sci. U.S.A.* **118**, e2108924118 (2021).
  - [5] R.-W. Zhang, C. Cui, R. Li, J. Duan, L. Li, Z.-M. Yu, and Y. Yao, Predictable gate-field control of spin in altermagnets with spin-layer coupling, *Phys. Rev. Lett.* **133**, 056401 (2024).
  - [6] L. Šmejkal, A. B. Hellenes, R. González-Hernández, J. Sinova, and T. Jungwirth, Giant and Tunneling Magnetoresistance in Unconventional Collinear Antiferromagnets with Nonrelativistic Spin-Momentum Coupling, *Phys. Rev. X* **12**, 011028 (2022).
  - [7] X.-Y. Hou, H.-C. Yang, Z.-X. Liu, P.-J. Guo, and Z.-Y. Lu, Large intrinsic anomalous Hall effect in both Nb<sub>2</sub>FeB<sub>2</sub> and Ta<sub>2</sub>FeB<sub>2</sub> with collinear antiferromagnetism, *Phys. Rev. B* **107**, L161109 (2023).
  - [8] P.-J. Guo, Z.-X. Liu, and Z.-Y. Lu, Quantum anomalous hall effect in collinear antiferromagnetism, *npj Comput. Mater.* **9**, 70 (2023).
  - [9] J. Krempaský, L. Šmejkal, S. W. D'Souza, M. Hajlaoui, G. Springholz, K. Uhlířová, F. Al Arab, P. C. Constantinou, V. Stokov, D. Usanov, W. R. Pudelko, R. González-Hernández, A. Birkhellenes, Z. Jansa, H. Reichlová, Z. Šobán, R. D. Gonzalez Betancourt, P. Wadley, J. Sinova, D. Kriegner, J. Minár, J. H. Dil, and T. Jungwirth, Alter magnetic lifting of kramers spin degeneracy, *Nature* **10.1038/s41586-023-06907-7** (2024).
  - [10] S. Reimers, L. Odenbreit, L. Šmejkal, V. N. Strocov, P. Constantinou, A. B. Hellenes, R. J. Ubierno, W. H. Campos, V. K. Bharadwaj, A. Chakraborty, T. Denneulin, W. Shi, R. E. Dunin-Borkowski, S. Das, M. Kläui, J. Sinova, and M. Jourdan, Direct observation of altermagnetic band splitting in CrSb thin films, *Nat Commun* **15**, 2116 (2024).
  - [11] C.-Y. Tan, Z.-F. Gao, H.-C. Yang, K. Liu, P.-J. Guo, and Z.-Y. Lu, Bipolarized weyl semimetals and quantum crystal valley hall effect in two-dimensional altermagnetic materials (2024), [arXiv:2406.16603 \[cond-mat.mtrl-sci\]](https://arxiv.org/abs/2406.16603).
  - [12] J. M. Luttinger and J. C. Ward, Ground-state energy of a many-fermion system. ii, *Phys. Rev.* **118**, 1417 (1960).
  - [13] W. Kohn and J. M. Luttinger, Ground-state energy of a many-fermion system, *Phys. Rev.* **118**, 41 (1960).
  - [14] J. M. Luttinger, Fermi surface and some simple equilibrium properties of a system of interacting fermions, *Phys. Rev.* **119**, 1153 (1960).
  - [15] Y. Liu, S.-D. Guo, Y. Li, and C.-C. Liu, Two-dimensional fully compensated ferrimagnetism, *Phys. Rev. Lett.* **134**, 116703 (2025).
  - [16] P.-J. Guo, X.-Y. Hou, Z.-F. Gao, H.-C. Yang, W. Ji, and Z.-Y. Lu, Luttinger compensated bipolarized magnetic semiconductor, *arXiv preprint arXiv:2502.18136* (2025), available at: <https://doi.org/10.48550/arXiv.2502.18136>.
  - [17] W. Kohn and L. J. Sham, Self-consistent equations including exchange and correlation effects, *Physical Review* **140**, A1133 (1965).
  - [18] P. Hohenberg and W. Kohn, Inhomogeneous electron gas, *Physical Review* **136**, B864 (1964).
  - [19] G. Kresse and J. Furthmüller, Efficient iterative schemes for ab initio total-energy calculations using a plane-wave basis set, *Physical Review B* **54**, 11169 (1996).
  - [20] G. Kresse and J. Hafner, Ab initio molecular dynamics for liquid metals, *Physical Review B* **47**, 558 (1993).
  - [21] G. Kresse and J. Furthmüller, Efficiency of ab-initio total energy calculations for metals and semiconductors using a plane-wave basis set, *Computational Materials Science* **6**, 15 (1996).
  - [22] G. Kresse and D. Joubert, From ultrasoft pseudopotentials to the projector augmented-wave method, *Physical Review B* **59**, 1758 (1999).
  - [23] J. P. Perdew, K. Burke, and M. Ernzerhof, Generalized gradient approximation made simple, *Physical Review Letters* **77**, 3865 (1996).
  - [24] N. Marzari, A. A. Mostofi, J. R. Yates, I. Souza, and D. Vanderbilt, Maximally localized wannier functions: Theory and applications, *Reviews of Modern Physics* **84**, 1419 (2012).
  - [25] V. I. Anisimov, J. Zaanen, and O. K. Andersen, Band theory and mott insulators: Hubbard u instead of stoner i, *Phys. Rev. B* **44**, 943 (1991).
  - [26] S. L. Dudarev, G. A. Botton, S. Y. Savrasov, C. J. Humphreys, and A. P. Sutton, Electron-energy-loss spectra and the structural stability of nickel oxide: An lsd+u study, *Phys. Rev. B* **57**, 1505 (1998).
  - [27] A. A. Mostofi, J. R. Yates, G. Pizzi, Y.-S. Lee, I. Souza, D. Vanderbilt, and N. Marzari, An updated version of wannier90: A tool for obtaining maximally-localised wannier functions, *Computer Physics Communications* **185**, 2309 (2014).
  - [28] E. Solana-Madruga, A. M. Arévalo-López, A. J. Dos santos García, C. Ritter, C. Cascales, R. Sáez-Puche, and J. P. Attfield, Anisotropic magnetic structures of the MnRMnSbO<sub>6</sub> high-pressure doubly ordered perovskites (R = La, Pr, and Nd), *Phys. Rev. B* **97**, 134408 (2018).
  - [29] E. Solana-Madruga, Á. M. Arévalo-López, A. J. Dos-Santos-García, E. Urones-Garrote, D. Ávila-Brandé, R. Sáez-Puche, and J. P. Attfield, Double double cation order in the high-pressure perovskites MnRMnSbO<sub>6</sub>, *Angew. Chem. Int. Ed.* **55**, 9340 (2016), the standard abbreviation for Angewandte Chemie International Edition is Angew. Chem. Int. Ed.